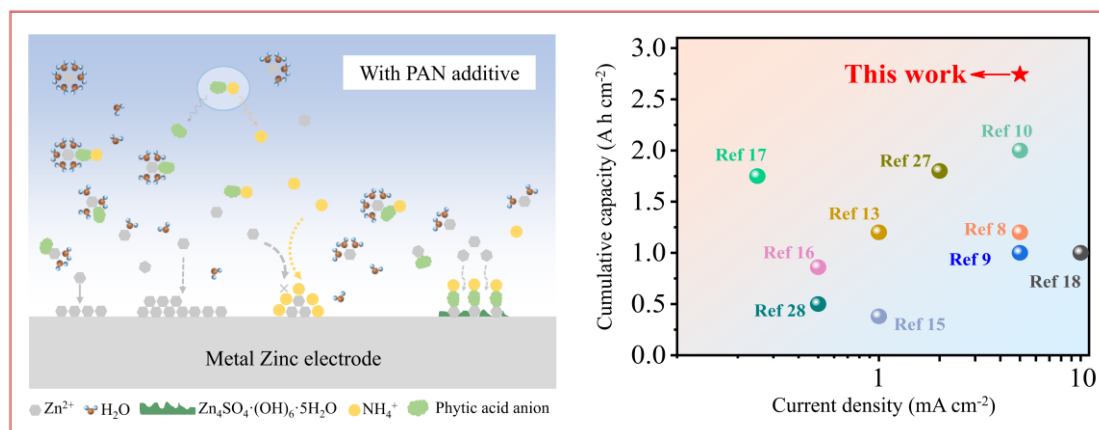


Graphic Abstract



Caption of Graphic Abstract

By introducing a minute quantity of phytate ammonium into the conventional dilute zinc sulfate electrolyte, a static physical barrier is established by the phytic anion. Simultaneously, a dynamic electrostatic shield layer collaborates, yielding superior electrochemical performance. This addition facilitates an accelerated de-solvation process, effectively suppressing the so-called "tip effect" and mitigating dendrite growth.

Zincophilic armor: Phytate ammonium as a multifunctional additive for enhanced performance in aqueous zinc-ion batteries

Fangyuan Xiao^{a,b}, Xiaoke Wang^{a,b}, Kaitong Sun^a, Qian Zhao^a, Cuiping Han^{b,*}, and Hai-Feng Li^{a,*}

^a*Institute of Applied Physics and Materials Engineering, University of Macau, Avenida da Universidade, Taipa, Macao SAR 999078, China*

^b*Faculty of Materials Science and Energy Engineering/Institute of Technology for Carbon Neutrality, Shenzhen Institute of Advanced Technology, Chinese Academy of Sciences, Shenzhen Guangdong 518055, China.*

Email addresses: cp.han@siat.ac.cn (C. Han)
haifengli@um.edu.mo (H.-F. Li)

Corresponding author: haifengli@um.edu.mo (H.-F. Li),
Full postal address:
IAPME, N23-3002, University of Macau
Avenida da Universidade, Taipa, Macao SAR 999078, China
Phone: +853 6307 5422

Abstract

Corrosion and the formation of by-products resulting from parasitic side reactions, as well as random dendrite growth, pose significant challenges for aqueous zinc-ion batteries (AZIBs). In this study, phytate ammonium is introduced into the traditional dilute Zinc sulfate electrolyte as a multi-functional additive. Leveraging the inherent zincophilic nature of the phytic anion, a protective layer is formed on the surface of the zinc anode. This layer can effectively manipulate the deposition process, mitigate parasitic reactions, and reduce the accumulation of detrimental by-products. Additionally, the competitive deposition between dissociated ammonium ions and Zn^{2+} promotes uniform deposition, thereby alleviating dendrite growth. Consequently, the modified electrolyte with a lower volume addition exhibits superior performance. The zinc symmetric battery demonstrates much more reversible plating/stripping, sustaining over 2000 hours at 5 mA cm^{-2} and 1 mA h cm^{-2} . A high average deposition/stripping efficiency of 99.83% is achieved, indicating the significant boosting effect and practical potential of our strategy for high-performance aqueous zinc-ion batteries.

Keywords: Zinc-ion battery, Anode, Electrolyte design, Effective additive

1. Introduction

Lithium-ion batteries (LIBs) have found widespread applications since their initial commercialization by SONY in 1991 [1]. The expanding market scale has led to rapid resource consumption, resulting in rising costs. Additionally, traditional commercial batteries often utilize organic compounds as solvents paired with polymer separators, posing a hidden danger of fire in the event of a short circuit or overheating. This risk is particularly pronounced when batteries are used in electric vehicles or other high-power facilities through series connection [2, 3]. Under extreme conditions, local overheating caused by a short circuit can lead to the decomposition of the organic electrolyte. As the temperature continues to rise, the battery may undergo firing and combustion, posing a threat to personal safety [4]. Zinc-ion batteries (ZIBs) emerge as promising candidates for the next generation of large-scale energy storage devices, offering a potential solution to the challenges faced by LIBs. Zinc metal boasts a high specific capacity (820 mA h g^{-1}) and an appropriate reduction potential (Zn^{2+}/Zn , -0.76 V vs. SHE), providing favorable compatibility with aqueous electrolyte [5-7]. By utilizing water as the electrolyte solvent, battery security can be greatly improved compared to traditional organic solvent electrolytes. However, challenges persist with aqueous electrolytes.

Traditional aqueous zinc sulfate (ZnSO_4) electrolytes suffer from several typical problems, which can be categorized into three parts: i) Dendrite growth caused by random zinc ion flux and deposition [8-11], significantly reducing the cell's lifespan. ii) By-product accumulation resulting from unexpected side reactions, where by-products typically consist of zinc hydroxyl sulfate (ZHS, $\text{Zn}_4\text{SO}_4(\text{OH})_6 \cdot n\text{H}_2\text{O}$). The accumulation of ZHS increases the interface resistance, hindering zinc ion transport and decreasing electrode reaction kinetics [12-14]. iii) Weakly acidic electrolytes inevitably corrode the metal anode and aggravate hydrogen evolution reactions (HER) simultaneously [15-18]. These facts result in extra metal consumption due to irreversible reactions, leading to the rapid degradation of the battery. Furthermore, continued corrosion and metal consumption generate gas without pressure relief and buffer, posing a danger of excessive flammable and explosive hydrogen gas accumulation in the sealing system. Additionally, some zinc ions tend to combine with H_2O to form hydrated zinc ions ($\text{Zn}(\text{6H}_2\text{O})^{2+}$) through a solvation process in a solution system. The larger ion size of $\text{Zn}(\text{6H}_2\text{O})^{2+}$ compared to bare Zn^{2+} shows down ion transference [19-22], and water molecules impede the de-solvation process, resulting in slower ion transport. The competitive reduction between Zn^{2+} and H^+ leads to severe side reactions with an acid electrolyte [23, 24]. These issues must be addressed before the practical application of AZIBs.

Numerous strategies have been proposed to address these challenges, including electrode modulation [25], electrode-electrolyte interface engineering [26], separator design [27], and electrolyte optimization [28, 29]. These approaches aim to regulate ion solvation structure and random deposition, thereby mitigating dendrite growth and unfavorable HER. Functional additives are garnering increasing research interest due to their low cost, ease of implementation, and high effectiveness [30-32]. Among various functional additives, organic molecules represent an important category [33-35]. For instance, Xie et al. [36] proposed polyacrylic acid (PAA) as an additive for a sol-containing electrolyte, resulting in the formation of an in-situ solid electrolyte interface and achieving exceptional battery life. Additionally, Sun [37] introduced MXene nanosheets into a typical electrolyte, leading to an enhanced lifespan through facilitated ion migration.

Ammonium ions have been proven to efficiently regulate the deposition behavior of Zn^{2+} by forming a dynamic electrostatic shielding layer on the zinc metal surface [38]. Ammonium ions adsorb at the tip/raised part of the metal surface, preventing subsequent vertical deposition of Zn^{2+} through their static shielding effect on the tip area. This slows down irregular deposition speed, ensuring a uniform deposition process. Phytic acid serves as a typical metal corrosion inhibitor and organic ligand, significantly improving the electrochemical performance of the zinc anode after treatment [39]. The improved performance results from the establishment of an artificial protection layer containing phytate zinc. Additionally, a special ion transfer mechanism is prompted, where a special electro-migration channel formed by phytic anion and zinc ion acts as an efficient pathway for fast ion transmission. The deposition energy barrier of zinc ions is reduced with surface modulation.

In this study, we developed an electrolyte engineering strategy using a multifunctional additive of phytate ammonium (PAN). On one hand, owing to the inherent zincophilicity of the phytic anion, a physical barrier composed of zinc salt with phytic is generated. This layer enhances the stability of the electrode-electrolyte interface, mitigates side reactions, and reduces the accumulation of by-products. On the other hand, the static electric shield of NH_4^+ suppresses the “tip effect” (dendrite growth from uneven deposition of zinc ions caused by the inhomogeneous distribution of the electric field) during the deposition process, achieving uniform deposition. With a small amount of PAN addition, the cyclic performance of diluted ZnSO_4 is remarkably improved. Benefiting from the mentioned merits, the lifespan of the $\text{Zn}||\text{Zn}$ symmetric battery improves nearly tenfold, from 155 hours to 1500 hours, with 1% volume multifunctional additive PAN at 1 mA cm^{-2} , 1 mA h cm^{-2} . A high average Coulombic efficiency of 99.83% is achieved within 2000 cycles of $\text{Zn}||\text{Cu}$ asymmetry battery, indicating favorable reversibility and cycle stability. A full battery paired with a typical

V₂O₅ cathode also exhibits acceptable capability, illustrating the practical application potential of this additive design.

2. Experimental

2.1. Materials

Phytic acid (C₆H₁₈O₂₄P₆, solution in water, 50 wt%), N-Methylpyrrolidone (NMP, 99.9%), and Zinc sulfate heptahydrate (ZnSO₄·7H₂O, AR) were purchased from Shanghai Aladdin Bio-chem Technology. Ammonia (NH₃·H₂O, 25% ~28%) was purchased from SINOPHARM, and Vanadium pentoxide (V₂O₅, 99.6%) was acquired from Alfa Aesar. Ketjen black was obtained from SUZHOU SINERO TECHNOLOGY, and PVDF 5120 was purchased from Guangdong Canrd New Energy Technology.

2.2. Electrolyte/ Electrode preparations

1M ZnSO₄·7H₂O solution was prepared in deionized water to create the pristine electrolyte, labeled as the ‘bare electrolyte’ (denoted as BE). For the additive, 65 μL of Phytic acid and 50 μL of Ammonia were added to 5 mL of deionized water, resulting in an additive denoted as ‘PAN’, with a pH value around 5.5. The modified electrolyte containing 1% PAN was prepared by adding a 1% volume ratio PAN solution to the bare electrolyte. Additionally, a series of electrolytes with varying PAN concentrations (0.5%, 2%, and 5% by volume) were prepared using the same procedure. All preparation steps were conducted at room temperature.

Commercial zinc foil with different thicknesses (10 μm, 20 μm, and 80 μm) was purchased, polished with sandpaper, and wiped with ethanol to remove the oxide layer and impurities. The processed zinc foil was cut into small pieces measuring 1 cm × 1 cm, which were used as electrodes for the symmetric battery and anode for the full battery. To prepare the cathode, commercial V₂O₅ (without any modification), Ketjen black, and PVDF were mixed with a mass ratio of 7: 2: 1 using an agate mortar, with NMP as the dispersant. The uniform slurry was then coated on a stainless steel (SS, 100 μm) foil with a surgery blade. After evaporating the dispersant in an oven at 80 °C for 12 hours, the resulting cathode was obtained, featuring an average mass loading of ~ 1 mg cm⁻² and an N/P ratio of ~ 28.4.

2.3. Characterizations

Microstructure images were obtained using a Scanning Electron Microscope (Zeiss Sigma FESEM) equipped with Energy Dispersive Spectroscopy (EDS, Oxford) for element analysis. Crystalline data of the electrodes were measured by X-ray diffractometer (Rigaku, SmartLab 9 kW), with copper as the anode target material and

output $K\alpha$ radiation at 1.5418 Å (containing $K\alpha_1 = 1.54056$ Å and $K\alpha_2 = 1.54439$ Å as the radiation with an intensity ratio of 2: 1). The two-theta degree range was from 5 to 60° with a scan rate of 10 °/min. The contact angle of the electrolyte with the metal foil was tested by a Drop Shape Analyzer (Ningbo Scientific Instruments, OSA100S-T-P). Binding energy information of the functional group with the electrode was detected by X-ray photoelectron spectroscopy (Thermo Fisher Scientific, ESCALAB250Xi).

2.4. Electrochemical measurements

Coin cells were assembled in CR2032 type, with zinc foil and glass fiber (GF/D, Whatman) used as anode and separator, respectively. Commercial V_2O_5 served as the cathode material for the full battery, with a 1M $ZnSO_4$ /1M $ZnSO_4$ +1% PAN electrolyte.

Long cycle performance was measured using the Neware battery test system (Shenzhen, China). Coulombic efficiency (CE) was tested by a Zn|| Cu asymmetric battery, used to estimate the plating/ stripping efficiency. Cyclic Voltammetry (CV), Chronoamperometry (CA), Linear Polarization (LP) test, and Electrochemical Impedance Spectroscopy (EIS) tests were analyzed using an Electrochemical Workstation (CH Instruments, CHI760E, Shanghai). For the CV test, the scan rate was 1 $mV s^{-1}$ with a voltage range from 0.2 to 1.9 V. CA curves were recorded with a -150 mV constant potential for 400 seconds. The potential range of Linear polarization was -0.2 V to 0.2 V with a scan rate of 1 $mV s^{-1}$. EIS was probed by the electrochemical workstation at a frequency range from 10 mHz to 100 kHz with an amplitude of 5 mV. All these tests were performed with coin cells at room temperature unless specially marked.

3. Results and discussion

3.1. Influence of PAN on the morphology of zinc anode

Fig. 1a presents a schematic illustrating some typical challenges associated with traditional dilute $ZnSO_4$ electrolytes. While the zinc metal anode boasts a high theoretical capacity, several difficulties hinder the widespread application of zinc-ion batteries on a large scale. These challenges include the slow kinetics of the de-solvation process from zinc hydrates to zinc ions, the formation of dendrites during random and uneven zinc ion deposition, surface passivation resulting from the accumulation of inert by-products, and simultaneous corrosion and hydrogen evolution reactions. Upon the addition of PAN, the cations and anions decomposed from PAN enhance the electrochemical performance in several ways: the phytic anion actively participates in the solvation process of zinc ions, adjusting the solvation structure for fast ion transportation. Simultaneously, a protective layer is formed, leveraging the intrinsic zincophilic properties of the phytic anions on zinc metal. This in-situ protection layer,

composed of phytate zinc, regulates ion flux for a uniform deposition process. Additionally, the additive mitigates side reactions and reduces by-product accumulation, alleviating random zinc deposition and dendrite growth by restraining the “tip effect” from ammonium ions. In Fig. 1b, the contact angle test results show that the pristine electrolyte without the addition has a contact angle of 85.6°, which decreases to 80.5° after the addition of PAN. This indicates that the additive improves wettability to the electrode, facilitating faster infiltration and contributing to the construction of a stable solid electrode interface, resulting in refined zinc crystal size during the deposition process. The surface morphology evolution of the electrode during aging is illustrated in Fig. 1c. After 20 hours (equivalent to 10 cycles at 1 mA cm⁻², 1 mA h cm⁻²), the electrode demonstrates a relatively flat and uniform surface. In contrast to the smooth surface of the zinc metal foil (Fig. S1a), micro-clusters and microspheres are observed on the zinc electrode when paired with the pristine electrolyte. These features are believed to be by-products of chemical corrosion (Fig. S1b). The superior anode consistency in the aging test demonstrates that the additive imparts better anti-corrosion ability to the zinc anode. At high magnification in the SEM images of the zinc electrode with the additive (Fig. S1c) and corresponding EDS mapping results (Fig. S1d), a dual defense mechanism is hypothesized to be established. This mechanism is derived from the synergistic function of phytic anions and ammonium ions: a protection layer formed by phytic anions and a dynamic electrostatic shield layer from the superior absorption of NH₄⁺. The uniform distribution of C and N elements on the metal surface suggests the presence of an in-situ protection layer. Cross-section images in Fig. S1e and Fig. S1f confirm the existence of this thin protection layer and its positive effect on electrode protection. Dissociated ammonium ions suppress the tip effect, extending the lifespan. X-ray diffraction results with the electrode from the aging battery support this conclusion. Besides the strong characteristic peaks from zinc metal after 35°, a single peak appears at 8.09° with both electrodes after aging (Fig. 1d), attributed to ZHS (Zn₄SO₄(OH)₆·5H₂O, JCPDS No. 78-0246). Due to the protection layer on the zinc metal anode surface, the intensity of this characteristic peak decreases after the addition of PAN, suggesting that PAN effectively reduces side reactions and by-product accumulation. To further confirm the influence of the additive, X-ray photoelectron spectroscopy (XPS) of the electrodes was surveyed, and the results are exhibited in Fig. 1e. The signals observed at 286.19 eV for C 1s and 532.37 eV for O 1s are attributed to the presence of the C-O bond originating from the phytic anion. The existence of the C-O bond on the electrode surface reveals that the additive is absorbed on the zinc metal surface due to its zincophilicity, consistent with the EDS mapping results in Fig. S1d. Additionally, a pair of S 2p peaks is detected in both samples (Fig. S2), illustrating that the cell still experiences some degree of side reactions, mainly caused by chemical

corrosion.

3.2. Electrochemical performance improvement

As shown in Fig. 2a, we assembled a Zn|| Zn symmetric battery for chronoamperometry test. The bare ZnSO₄ electrolyte exhibits a prolonged time to achieve a stable current density, typically described as a two-dimensional (2D) diffusion behavior, as illustrated in the insert scheme in Fig. 2a. In this scenario, zinc ion flux and deposition concentrate on a 2D plane, leading to vertical growth and the formation of dendrites that can damage the separator, potentially causing short circuits. After adding the PAN additive, the corresponding current density stabilizes in less than 50 seconds, attributed to a three-dimensional diffusion model. Zinc ions preferentially deposit on the surface in a parallel mode, promoting uniform deposition and reducing dendrite formation. The linear polarization test results depicted in Fig. 2b illustrate the anodic/cathodic polarization process, simulating the Tafel slope and calculating the corrosion current for different electrolytes. It is observed that the corrosion current decreases from 0.87 mA to 0.51 mA after adding of PAN. Although the additive is weakly acidic, the corrosion potential remains basically unchanged, confirming that the additive does not exacerbate corrosion and hydrogen evolution reaction (HER). Cyclic voltammetry of the symmetric battery in Fig. S3a depicts a lower overpotential after addition, revealing reduced resistance and energy barrier, facilitating an easier zinc ion deposition process. The electrochemical impedance spectra of the symmetry battery paired with electrolytes containing varying amounts of the additive are illustrated in Fig. S3b, and S3c. The lowest charge transfer resistance is observed with a 1% volume addition, establishing it as the optimal amount for subsequent research. At 1 mA cm⁻² and an area capacity of 1 mA h cm⁻², the symmetry battery with the bare electrolyte fails within 155 hours (Fig. 2c). In contrast, the electrolyte with the additive demonstrates stable cycling performance for more than 1500 hours, with a voltage hysteresis of only 13.9 mV after 1200 hours, indicating high reversibility and an efficient stripping/deposition process. The rating performance of the symmetric battery in Fig. 2d, applied at 1 mA h cm⁻² with series current densities of 1, 2, 5, 10, and 20 mA cm⁻², respectively, maintains stable cycling performance even at high current densities, with the voltage hysteresis at different current densities lower than that without the additive, verifying the improvement of PAN addition to rating performance. A Zn|| Cu asymmetric battery is typically assembled to assess Coulombic efficiency (CE). In Fig. 2e, Coulombic efficiency of bare ZnSO₄ electrolyte fluctuates 100 % after 500 cycles, with a distinct fluctuation observed around 1000 cycles (see insert picture on Fig. 2e). In contrast, the electrolyte with the additive maintains good reversibility even after 2000 cycles, confirming that PAN addition enables a much more stable deposition process.

The results reveal a high initial Coulombic efficiency (97.3%) and a higher average Coulombic efficiency of 99.83% after 2000 cycles, superior to many former reports under the same condition (Fig. 2f) [40, 41]. Compared with the bare ZnSO₄ electrolyte (Fig. 2g), the nucleation overpotential (NOP) decreases to 16.6 mV after the addition of PAN. The lowered NOP indicates a lower nucleation barrier and an improved interfacial activity, suggesting that PAN addition allows for better nucleation kinetics. Additionally, as shown in the voltage capacity curve in Fig. 2h and Fig S4, the polarization overpotential profit reduces from 91 mV to 74 mV and maintains a similar value in the first 100 cycles. Well-overlapped voltage curves also indicate good anode stability and reversibility. The electrochemical performance test results above imply the effective function of the PAN additive in implementing a better lifespan of the zinc anode.

Further investigation reveals the enhanced performance of the electrolyte with PAN additive. The Zn||Zn symmetric battery demonstrated an extremely stable cyclic performance (over 2000 hours) at a current density of 5 mA cm⁻², 1 mA h cm⁻². It also exhibited a low voltage hysteresis during the long-term charge and discharge process (Fig. 3a), attributed to the adjustment of the solvation structure of Zn²⁺ and a more ordered ion flux. In contrast, the symmetric battery with bare ZnSO₄ electrolyte suffered a short circuit at 190 hours due to a large over-potential, water involvement side reactions, and the formation of low ionic conductivity by-products, leading to a faulty anode surface and rapid battery failure. Depth of discharge (DOD) is an important standard reflecting the utilization of the metal anode, with a higher DOD approaching practical conditions. When the DOD increased to 21.3%, the cell smoothly ran for over 1000 hours with a lower over-potential, as Figure. S5a shows. At a large DOD of 42.6% in Fig. 3b, the battery could still maintain steady performance for more than 160 hours. Even at a specific high level to 51.1%, a stable cycle of more than 150 hours could also be realized (Fig. S5b), providing the practical value of our design. As Fig. 3c displays, the as-assembled coin cell obtained a cumulative capacity of more than 2700 mA h cm⁻² at the current density of 5 mA cm⁻² [42, 43]. The improvement in cumulative capacity in this work is remarkable compared with other studies.

3.3. Alleviated the accumulation of by-products and enhanced zinc ion dynamics

To explore the instant influence of the PAN addition on the charge/discharge process, morphology, and crystalline details of the electrode after short-term cycles are gathered. From the X-ray diffraction results (Fig. 3d) of the electrode after ten cycles, compared with the Zinc plate paired with PAN additive, the electrode with bare electrolyte shows a stronger characteristic peak of ZHS at 8.09 ° than that with the additive. The physical barrier built with the phytic anion could alleviate the

accumulation of $\text{Zn}_4\text{SO}_4(\text{OH})_6 \cdot 5\text{H}_2\text{O}$ to a certain extent and regulate an even Zn^{2+} ion flux. Furthermore, after 10 cycles, optical image (inserted in Fig. S6a, S6b) also reveal a noticeable difference: a darker and more homogeneous electrode surface was obtained after the addition, indicating modification of the electrode surface. Messy deposited Zn and a large amount of ZHS could be noticed on the Zn plate surface (Fig. S6a). This is in stark contrast to the neat and flat surface of the electrode paired with the modified electrolyte (Fig. S6b and S6c), demonstrating the positive effect of the PAN additive in ameliorating the accumulation of ZHS. XPS results in Fig. 3e evidenced a similar result: the S 2p orbit splitting signal on 168 eV is detected on the Zn plate paired with BE electrolyte after 10 cycles. However, there is no obvious response of the S 2p orbit splitting on the electrode surface after addition, turned out a low-level accumulation of ZHS than the bare electrolyte. Additionally, a C-O bond could be found on the fine spectrum of C 1s and O 1s after the cycle (Fig. S7a), which is in consistent with previous results of the aged battery of a protection layer hypothesis. In addition, nitrogen signals of N 1s are also discovered from the aged and cycled battery with PAN additive (Fig. S7b). It is believed that the corresponding peak belongs to NH_4^+ of the residue of PAN. The corresponding N 1s peak is detected in the addition sample before the cycle, too. This furtherly confirms the existence of the protection layer. Furthermore, according to previous reports [38], there exists a competitive absorption phenomenon between dissociated NH_4^+ and Zn^{2+} during the deposition process. NH_4^+ tends to be preferentially absorbed onto the surface, thereby forming an electrostatic shield on protuberant areas. Electrostatic repulsion will stop the subsequent deposition and compel zinc ions to plate in the nearby area, which could effectively inhibit the vertical deposition of zinc ions and then alleviate the random dendrite growth. Ammonium phytate will also undergo partial dissociation in solution. It is speculated that the static electric shield layer containing NH_4^+ has formed in the deposition process, too, promoting reversibility and lifespan.

Electrochemical impedance spectroscopy (EIS) was also utilized to elucidate the migration of zinc ions during the charge and discharge process. As shown if Fig. 3f, using the inert picture as a reference model, the electrochemical impedance of the symmetric battery with 1M ZnSO_4 as the electrolyte was measured to be 425 Ω . Upon the addition of 1% vol PAN, the electrochemical impedance prior to cycling decreased to 100 Ω . Faster ion transfer and better reaction kinetics are obtained with the functional addition. By combining the Chronamperometry (CA) technique with electrochemical impedance spectroscopy testing, we can estimate the ion transference number of the symmetric battery with different electrolytes [44]. The ion transference number follows:

$$T = \frac{I_s(\Delta V - I_0 R_0)}{I_0(\Delta V - I_s R_s)}, \quad (1)$$

where T represent the zinc ion transference number, I_0 is the initial current, I_s

corresponds the steady-state current, R_0 and R_s refer to the resistance of the initial and steady states, ΔV is the amplitude (applied with 5 mV). The EIS results before and after the addition are depicted in Fig. 3g, where the electrolyte with the functional additive delivers a lower charge transfer resistance of 117.4 Ω compared to that with the bare electrolyte (412.8 Ω) based on the model (insert in Fig. 3f) simulation results. Calculated with the equation above, the zinc ion transference number increased from 0.41 to 0.595 after the addition. A higher ion transference number represents a more rapid ion migration, which is indispensable for a uniform electric field distribution and even deposition of zinc ions. The result confirms a more efficient ion transport with the adjustment of the solvation structure from the phytic anion. Activation energy (E_a) is an important parameter that reflects the de-solvation energy barrier [45]; it can be calculated with the:

$$\ln \frac{1}{R_{ct}} = \frac{E_a}{RT}, \quad (2)$$

where R_{ct} represents the charge transfer resistance, E_a represents activation energy, $R = 8.314 \text{ J}/(\text{mol}\cdot\text{K})$ is the gas constant, and T is temperature in Kelvin. EIS data from 10 $^{\circ}\text{C}$ to 60 $^{\circ}\text{C}$ is presented in Fig. 3g and Fig S8, and the cell with a modified electrolyte exhibits lower charge transfer resistance at each temperature condition. There is a liner relationship between $\ln (1/ R_{ct})$ and $1/ T$ (Fig. 3h). Calculations with the formula yield the activation energy results. The activation energy of the bare electrolyte is 23.82 kJ mol^{-1} , it reduces to 15.35 kJ mol^{-1} after adding the additive, indicating a lower de-solvation barrier and faster de-solvation process, attributed to the weakened solvation effect of H_2O after the phytic anion addition. Phytic ion and ammonium ion work synergistically to achieve a faster, uniform ion flux, well-distributed deposition of Zinc ions, and mitigated side reaction.

3.4. Practical application

A full battery with the typical cathode material vanadium oxide (V_2O_5) is assembled to further evaluate the effect of the PAN additive in a practical scale. Bare 1M ZnSO_4 and that with the additive serve as electrolyte for the full battery, respectively. The cyclic voltammetry (CV) results (first three cycles) of the assembled full battery are displayed in Fig. 4a and Fig. S9. Two pairs of redox peaks are observed, with two cathodic peaks at 0.9 V and 0.45~0.5 V marked as C_1 and C_2 , respectively, attributed to the co-insertion of $\text{Zn}^{2+}/\text{H}^+$, and corresponding anodic peaks marked as A_1 and A_2 represent the extraction of $\text{Zn}^{2+}/\text{H}^+$. Solid electrolyte interface (SEI) formation in the first cycle results in higher polarization, then the polarization potential of both redox peaks decreases. As the cycles continue, the reaction tends to be more stable and reversible, as illustrated by overlapping curves. The long-term cyclic performance of $\text{Zn}||\text{V}_2\text{O}_5$ full battery is displayed in Fig. 4b, where the discharge capacity of the commercialized V_2O_5 cathode reaches 115.2 mA h g^{-1} in the first cycle. As the cell

activates gradually, the specific capacity rises to 167.1 mA h g⁻¹ once and remains 65.9 mA h g⁻¹ after 200 cycles, achieving a high Coulombic efficiency of 99.8 %. Galvanostatic charge and discharge (GCD) profiles measured at 2 A g⁻¹ show a charge plateau around 1.24 V and a discharge plateau at nearly 0.89 V in the early cycles, with another discharge plateau around 0.52 V detected in subsequent cycles, consistent with the results of CV curves. The rating capability for the full battery with the PAN additive is shown in Fig. 4d, with an average charge capacity of 102.8, 106.5, 83.3, and 60.6 mA h g⁻¹ when applied at 1.0, 2.0, 5.0, and 10 A g⁻¹, respectively. As the current density is set back to 2.0 A g⁻¹, the specific capacity recovers to 113.3 mA h g⁻¹ without obvious capacity fade, demonstrating exceptional performance and reversibility at high current density. Electrochemical impedance spectroscopy of the full battery before cycling are displayed in Fig. 4e. According to the model (inserted at Fig. 4e, where R₁ refers to solution resistance, CPE represents Constant Phase Angle Element, R₂ is charge transfer resistance, and Wo is the Warburg Element) simulation results, charge transfer resistance (R_{ct}) of the full battery has decreased from 100.4 Ω to 27.86 Ω after the addition, illustrating the acceleration of ion transference and better reaction kinetics with the small amount additive.

4. Conclusions

In summary, we have proposed a simple and feasible strategy to enhance the stability of the zinc anode when applied with a traditional dilute ZnSO₄ electrolyte. By harnessing the intrinsic chelating ability of the phytic anion and its affinity for Zn²⁺, we modified the solvation structure of Zn²⁺ and achieved a uniform deposition process, thereby significantly enhancing ion transport efficiency. Furthermore, the restrain of tip effects from NH₄⁺ could alleviate dendrite growth. Benefiting from the synergistic effect of the additive, the electrochemical performance of the dilute ZnSO₄ electrolyte has been effectively enhanced. The Zn|| Zn symmetric battery sustained a long cyclic lifespan of more than 2000 hours at 1 mA h cm⁻² and exhibited a high average plating/stripping Coulombic efficiency of 99.83%. It also demonstrated superior cyclic stability for more than 150 hours at a high DOD of 51.1%. The full battery with V₂O₅ displayed acceptable cycle performance and stability. We believe our findings could provide a reference and inspire future research in the field of aqueous zinc-ion batteries.

CRedit authorship contribution statement

Fangyuan Xiao: Conceptualization, Methodology, Investigation, Data curation, Writing – original draft, Validation, Visualization. **Xiaoke Wang:** Investigation, Data curation. **Kaitong Sun:** Investigation, Data curation. **Qian Zhao:** Investigation, Data curation. **Cuiping Han:** Conceptualization, Methodology, Writing – review & editing,

Funding acquisition, Visualization, Supervision. **Hai-Feng Li:** Conceptualization, Methodology, Writing – review & editing, Funding acquisition, Visualization, Supervision.

Declaration of Competing Interest

The authors declare that they have no known competing financial interests or personal relationships that could have appeared to influence the work reported in this paper.

Data availability

Data will be made available on request.

Acknowledgements

The work at Shenzhen Institute of Advanced Technology was supported by Shenzhen Science and Technology Program (Grant No. RCYX20221008092934093). The work at University of Macau was supported by the Science and Technology Development Fund, Macao SAR (File Nos. 0090/2021/A2 and 0049/2021/AGJ), University of Macau (MYRG2020-00278-IAPME), and the Guangdong-Hong Kong-Macao Joint Laboratory for Neutron Scattering Science and Technology (Grant No. 2019B121205003).

Appendix A. Supplementary data

Supplementary data associated with this article can be found in the Elsevier Library or from the author. Supplementary data to this article can be found online at

References

- [1] Y. Nishi, Lithium ion secondary batteries; past 10 years and the future, *Journal of Power Sources* 100(1) (2001) 101-106. [https://doi.org/10.1016/S0378-7753\(01\)00887-4](https://doi.org/10.1016/S0378-7753(01)00887-4).
- [2] H. Pan, Y.-S. Hu, L. Chen, Room-temperature stationary sodium-ion batteries for large-scale electric energy storage, *Energy & Environmental Science* 6(8) (2013) 2338-2360. <https://doi.org/10.1039/C3EE40847G>.
- [3] B. Dunn, H. Kamath, J.-M. Tarascon, Electrical Energy Storage for the Grid: A Battery of Choices, *Science* 334(6058) (2011) 928-935. <https://doi.org/10.1126/science.1212741>.
- [4] X. Feng, S. Zheng, D. Ren, X. He, L. Wang, H. Cui, X. Liu, C. Jin, F. Zhang, C. Xu, H. Hsu, S. Gao, T. Chen, Y. Li, T. Wang, H. Wang, M. Li, M. Ouyang, Investigating the thermal runaway mechanisms of lithium-ion batteries based on thermal analysis database, *Applied Energy* 246 (2019) 53-64. <https://doi.org/10.1016/j.apenergy.2019.04.009>.
- [5] G. Liang, B. Liang, A. Chen, J. Zhu, Q. Li, Z. Huang, X. Li, Y. Wang, X. Wang, B. Xiong, X. Jin, S. Bai, J. Fan, C. Zhi, Development of rechargeable high-energy hybrid zinc-iodine aqueous batteries exploiting reversible chlorine-based redox reaction, *Nature Communications* 14(1) (2023) 1856. <https://doi.org/10.1038/s41467-023-37565-y>.
- [6] G. Liang, C. Zhi, A reversible Zn-metal battery, *Nature Nanotechnology* 16(8) (2021) 854-855. <https://doi.org/10.1038/s41565-021-00908-1>.
- [7] J. Hao, B. Li, X. Li, X. Zeng, S. Zhang, F. Yang, S. Liu, D. Li, C. Wu, Z. Guo, An In-Depth Study of Zn Metal Surface Chemistry for Advanced Aqueous Zn-Ion Batteries, *Advanced Materials* 32(34) (2020) 2003021. <https://doi.org/10.1002/adma.202003021>.
- [8] Y. Zhang, X. Han, R. Liu, Z. Yang, S. Zhang, Y. Zhang, H. Wang, Y. Cao, A. Chen, J. Sun, Manipulating the Zinc Deposition Behavior in Hexagonal Patterns at the Preferential Zn (100) Crystal Plane to Construct Surficial Dendrite-Free Zinc Metal Anode, *Small* 18(7) (2022) 2105978. <https://doi.org/10.1002/sml.202105978>.
- [9] K. Zhao, G. Fan, J. Liu, F. Liu, J. Li, X. Zhou, Y. Ni, M. Yu, Y.-M. Zhang, H. Su, Q. Liu, F. Cheng, Boosting the Kinetics and Stability of Zn Anodes in Aqueous Electrolytes with Supramolecular Cyclodextrin Additives, *Journal of the American Chemical Society* 144(25) (2022) 11129-11137. <https://doi.org/10.1021/jacs.2c00551>.

- [10] S. Zhang, M. Ye, Y. Zhang, Y. Tang, X. Liu, C.C. Li, Regulation of Ionic Distribution and Desolvation Activation Energy Enabled by In Situ Zinc Phosphate Protective Layer toward Highly Reversible Zinc Metal Anodes, *Advanced Functional Materials* 33(22) (2023) 2208230. <https://doi.org/10.1002/adfm.202208230>.
- [11] Z. Liu, J. Ma, X. Liu, H. Wu, D. Wu, B. Chen, P. Huang, Y. Huang, L. Wang, Z. Li, S. Chou, Coordinating zincophilic sites and a solvation shell for a dendrite-free Zn anode under the synergistic effects of polyacrylonitrile and dimethyl sulfoxide, *Chemical Science* 14(8) (2023) 2114-2122. <https://doi.org/10.1039/D2SC06276C>.
- [12] H. Chen, C. Dai, F. Xiao, Q. Yang, S. Cai, M. Xu, H.J. Fan, S.-J. Bao, Reunderstanding the Reaction Mechanism of Aqueous Zn–Mn Batteries with Sulfate Electrolytes: Role of the Zinc Sulfate Hydroxide, *Advanced Materials* 34(15) (2022) 2109092. <https://doi.org/10.1002/adma.202109092>.
- [13] T. Chen, F. Huang, Y. Wang, Y. Yang, H. Tian, J.M. Xue, Unveiling the Synergistic Effect of Ferroelectric Polarization and Domain Configuration for Reversible Zinc Metal Anodes, *Advanced Science* 9(14) (2022) 2105980. <https://doi.org/10.1002/advs.202105980>.
- [14] H. Peng, C. Liu, N. Wang, C. Wang, D. Wang, Y. Li, B. Chen, J. Yang, Y. Qian, Intercalation of organics into layered structures enables superior interface compatibility and fast charge diffusion for dendrite-free Zn anodes, *Energy & Environmental Science* 15(4) (2022) 1682-1693. <https://doi.org/10.1039/D1EE03624F>.
- [15] T. Wu, C. Ji, H. Mi, F. Guo, G. Guo, B. Zhang, M. Wu, Construction of zwitterionic osmolyte-based hydrogel electrolytes towards stable zinc anode for durable aqueous zinc ion storage and integrated electronics, *Journal of Materials Chemistry A* 10(48) (2022) 25701-25713. <https://doi.org/10.1039/D2TA07410A>.
- [16] K. Su, J. Chen, X. Zhang, J. Feng, Y. Xu, Y. Pu, C. Wang, P. Ma, Y. Wang, J. Lang, Inhibition of zinc dendrites by dopamine modified hexagonal boron nitride electrolyte additive for zinc-ion batteries, *Journal of Power Sources* 548 (2022) 232074. <https://doi.org/10.1016/j.jpowsour.2022.232074>.
- [17] G. Li, X. Wang, S. Lv, J. Wang, X. Dong, D. Liu, Long-life and low-polarization Zn metal anodes enabled by a covalent triazine framework coating, *Chemical Engineering Journal* 450 (2022) 138116. <https://doi.org/10.1016/j.cej.2022.138116>.
- [18] Q. Cao, Z. Pan, Y. Gao, J. Pu, G. Fu, G. Cheng, C. Guan, Stable Imprinted Zincophilic Zn Anodes with High Capacity, *Advanced Functional Materials* 32(41) (2022) 2205771. <https://doi.org/10.1002/adfm.202205771>.
- [19] T.C. Li, Y. Lim, X.L. Li, S. Luo, C. Lin, D. Fang, S. Xia, Y. Wang, H.Y. Yang, A

- Universal Additive Strategy to Reshape Electrolyte Solvation Structure toward Reversible Zn Storage, *Advanced Energy Materials* 12(15) (2022) 2103231. <https://doi.org/10.1002/aenm.202103231>.
- [20] D. Xie, Z.-W. Wang, Z.-Y. Gu, W.-Y. Diao, F.-Y. Tao, C. Liu, H.-Z. Sun, X.-L. Wu, J.-W. Wang, J.-P. Zhang, Polymeric Molecular Design Towards Horizontal Zn Electrodeposits at Constrained 2D Zn²⁺ Diffusion: Dendrite-Free Zn Anode for Long-Life and High-Rate Aqueous Zinc Metal Battery, *Advanced Functional Materials* 32(32) (2022) 2204066. <https://doi.org/10.1002/adfm.202204066>.
- [21] J.-H. Wang, W.-X. Dong, J. Chen, L.-F. Chen, Three-dimensional synergistic ionic-electronic conductor host assisted high-performance Zn metal battery, *Ionics* 29(8) (2023) 3097-3107. <https://doi.org/10.1007/s11581-023-05054-3>.
- [22] C. Meng, W. He, L. Jiang, Y. Huang, J. Zhang, H. Liu, J.-J. Wang, Ultra-Stable Aqueous Zinc Batteries Enabled by β -Cyclodextrin: Preferred Zinc Deposition and Suppressed Parasitic Reactions, *Advanced Functional Materials* 32(47) (2022) 2207732. <https://doi.org/10.1002/adfm.202207732>.
- [23] J. Zhu, Z. Bie, X. Cai, Z. Jiao, Z. Wang, J. Tao, W. Song, H.J. Fan, A Molecular-Sieve Electrolyte Membrane enables Separator-Free Zinc Batteries with Ultralong Cycle Life, *Advanced Materials* 34(43) (2022) 2207209. <https://doi.org/10.1002/adma.202207209>.
- [24] J. Yu, X. Jia, J. Peng, T. Wang, H. Feng, B. Meng, J. Zhao, N. Yang, Stable Zn-Ion Hybrid Supercapacitor Zinc Anode Achieved by Artificial Protective Layer of Nitrogen-Sulfur Co-Doping Activated Carbon, *Journal of The Electrochemical Society* 170(2) (2023). <https://doi.org/10.1149/1945-7111/acb66e>.
- [25] B. Li, S. Liu, Y. Geng, C. Mao, L. Dai, L. Wang, S.C. Jun, B. Lu, Z. He, J. Zhou, Achieving Stable Zinc Metal Anode Via Polyaniline Interface Regulation of Zn Ion Flux and Desolvation, *Advanced Functional Materials* 34(5) (2024) 2214033. <https://doi.org/10.1002/adfm.202214033>.
- [26] J. Cao, D. Zhang, Y. Yue, R. Chanajaree, S. Wang, J. Han, X. Zhang, J. Qin, Y. Huang, Regulating solvation structure to stabilize zinc anode by fastening the free water molecules with an inorganic colloidal electrolyte, *Nano Energy* 93 (2022) 106839. <https://doi.org/10.1016/j.nanoen.2021.106839>.
- [27] Y. Song, P. Ruan, C. Mao, Y. Chang, L. Wang, L. Dai, P. Zhou, B. Lu, J. Zhou, Z. He, Metal–Organic Frameworks Functionalized Separators for Robust Aqueous Zinc-Ion Batteries, *Nano-Micro Letters* 14(1) (2022) 218. <https://doi.org/10.1007/s40820-022-00960-z>.
- [28] J. Cao, Y. Sun, D. Zhang, D. Luo, L. Zhang, R. Chanajaree, J. Qin, X. Yang, J. Lu, Interfacial Double-Coordination Effect Guiding Uniform Electrodeposition for Reversible Zinc Metal Anode, *Advanced Energy Materials* 14(2) (2024) 2302770.

- <https://doi.org/10.1002/aenm.202302770>.
- [29] J. Cao, X. Wang, D. Zhang, R. Chanajaree, L. Zhang, J. Qin, X. Yang, Boosting Zn metal anode stability with a dimethylformamide additive, *Journal of Alloys and Compounds* 972 (2024) 172773. <https://doi.org/10.1016/j.jallcom.2023.172773>.
- [30] Z. Peng, Y. Li, P. Ruan, Z. He, L. Dai, S. Liu, L. Wang, S. Chan Jun, B. Lu, J. Zhou, Metal-organic frameworks and beyond: The road toward zinc-based batteries, *Coordination Chemistry Reviews* 488 (2023) 215190. <https://doi.org/10.1016/j.ccr.2023.215190>.
- [31] J. Cao, D. Zhang, X. Zhang, Z. Zeng, J. Qin, Y. Huang, Strategies of regulating Zn²⁺ solvation structures for dendrite-free and side reaction-suppressed zinc-ion batteries, *Energy & Environmental Science* 15(2) (2022) 499-528. <https://doi.org/10.1039/D1EE03377H>.
- [32] P. Zhou, K. Sun, S. Ji, Z. Zhao, Y. Fu, J. Xia, S. Wu, Y. Zhu, K. N. Hui, H.-F. Li, MgF₂ as an effective additive for improving ionic conductivity of ceramic solid electrolytes, *Materials Today Energy* 32 (2023) 101248. <https://doi.org/10.1016/j.mtener.2023.101248>.
- [33] Y. Du, Y. Li, B.B. Xu, T.X. Liu, X. Liu, F. Ma, X. Gu, C. Lai, Electrolyte Salts and Additives Regulation Enables High Performance Aqueous Zinc Ion Batteries: A Mini Review, *Small* 18(43) (2022) 2104640. <https://doi.org/10.1002/sml.202104640>.
- [34] X. Gu, Y. Du, Z. Cao, F. Ma, J. Li, Q. Wang, C. Lai, Hexamethylenetetramine additive with zincophilic head and hydrophobic tail for realizing ultra-stable Zn anode, *Chemical Engineering Journal* 460 (2023) 141902. <https://doi.org/10.1016/j.cej.2023.141902>.
- [35] C. Wu, C. Sun, K. Ren, F. Yang, Y. Du, X. Gu, Q. Wang, C. Lai, 2-methyl imidazole electrolyte additive enabling ultra-stable Zn anode, *Chemical Engineering Journal* 452 (2023) 139465. <https://doi.org/10.1016/j.cej.2022.139465>.
- [36] K. Xie, K. Ren, Q. Wang, Y. Lin, F. Ma, C. Sun, Y. Li, X. Zhao, C. Lai, In situ construction of zinc-rich polymeric solid–electrolyte interface for high-performance zinc anode, *eScience* 3(4) (2023) 100153. <https://doi.org/10.1016/j.esci.2023.100153>.
- [37] C. Sun, C. Wu, X. Gu, C. Wang, Q. Wang, Interface Engineering via Ti₃C₂T_x MXene Electrolyte Additive toward Dendrite-Free Zinc Deposition, *Nano-Micro Letters* 13(1) (2021) 89. <https://doi.org/10.1007/s40820-021-00612-8>.
- [38] D. Han, Z. Wang, H. Lu, H. Li, C. Cui, Z. Zhang, R. Sun, C. Geng, Q. Liang, X. Guo, Y. Mo, X. Zhi, F. Kang, Z. Weng, Q.-H. Yang, A Self-Regulated Interface toward Highly Reversible Aqueous Zinc Batteries, *Advanced Energy Materials* 12(9) (2022) 2102982. <https://doi.org/10.1002/aenm.202102982>.

- [39] H. Liu, J.-G. Wang, W. Hua, L. Ren, H. Sun, Z. Hou, Y. Huyan, Y. Cao, C. Wei, F. Kang, Navigating fast and uniform zinc deposition via a versatile metal–organic complex interphase, *Energy & Environmental Science* 15(5) (2022) 1872-1881. <https://doi.org/10.1039/d2ee00209d>.
- [40] K. Wang, T. Qiu, L. Lin, X.-X. Liu, X. Sun, A low fraction electrolyte additive as interface stabilizer for Zn electrode in aqueous batteries, *Energy Storage Materials* 54 (2023) 366-373. <https://doi.org/10.1016/j.ensm.2022.10.029>.
- [41] Y. Liu, Y. An, L. Wu, J. Sun, F. Xiong, H. Tang, S. Chen, Y. Guo, L. Zhang, Q. An, L. Mai, Interfacial Chemistry Modulation via Amphoteric Glycine for a Highly Reversible Zinc Anode, *ACS Nano* 17(1) (2023) 552-560. <https://doi.org/10.1021/acsnano.2c09317>.
- [42] W. Zhou, T. Wu, M. Chen, Q. Tian, X. Han, X. Xu, J. Chen, Wood-based electrodes enabling stable, anti-freezing, and flexible aqueous zinc-ion batteries, *Energy Storage Materials* 51 (2022) 286-293. <https://doi.org/10.1016/j.ensm.2022.06.056>.
- [43] Y. Liu, H. He, A. Gao, J. Ling, F. Yi, J. Hao, Q. Li, D. Shu, Fundamental study on Zn corrosion and dendrite growth in gel electrolyte towards advanced wearable Zn-ion battery, *Chemical Engineering Journal* 446 (2022) 137021. <https://doi.org/10.1016/j.cej.2022.137021>.
- [44] Q. He, G. Fang, Z. Chang, Y. Zhang, S. Zhou, M. Zhou, S. Chai, Y. Zhong, G. Cao, S. Liang, A. Pan, Building Ultra-Stable and Low-Polarization Composite Zn Anode Interface via Hydrated Polyzwitterionic Electrolyte Construction, *Nano-Micro Letters* 14(1) (2022) 93. <https://doi.org/10.1007/s40820-022-00835-3>.
- [45] C. Ma, K. Yang, S. Zhao, Y. Xie, C. Liu, N. Chen, C. Wang, D. Wang, D. Zhang, Z.X. Shen, F. Du, Recyclable and Ultrafast Fabrication of Zinc Oxide Interface Layer Enabling Highly Reversible Dendrite-Free Zn Anode, *ACS Energy Letters* 8(2) (2023) 1201-1208. <https://doi.org/10.1021/acsenergylett.2c02735>.

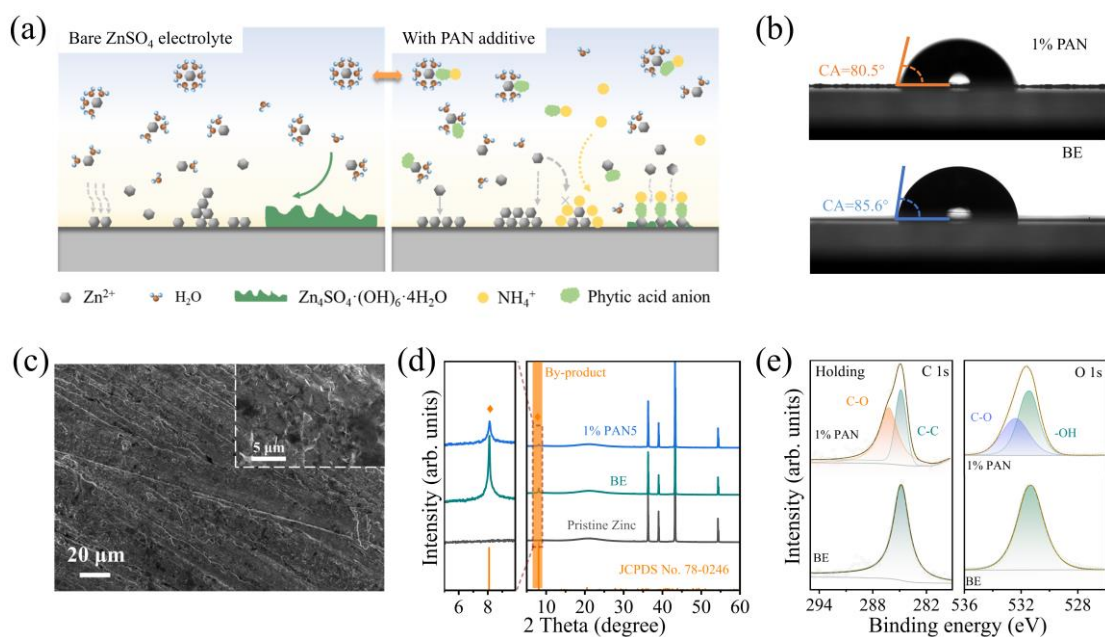


Fig. 1. a) Schematic of the primary challenges for the study of zinc-metal anode and function of the PAN additive. b) Contact angle test of bare electrolyte with and without the additive. c) SEM images of the zinc-metal anode with PAN after aging for 20 hours. d) XRD patterns of the zinc-metal anode before and after aging, e) Fine spectra from XPS survey around C 1s and O 1s edges of BE and with the PAN additive after aging.

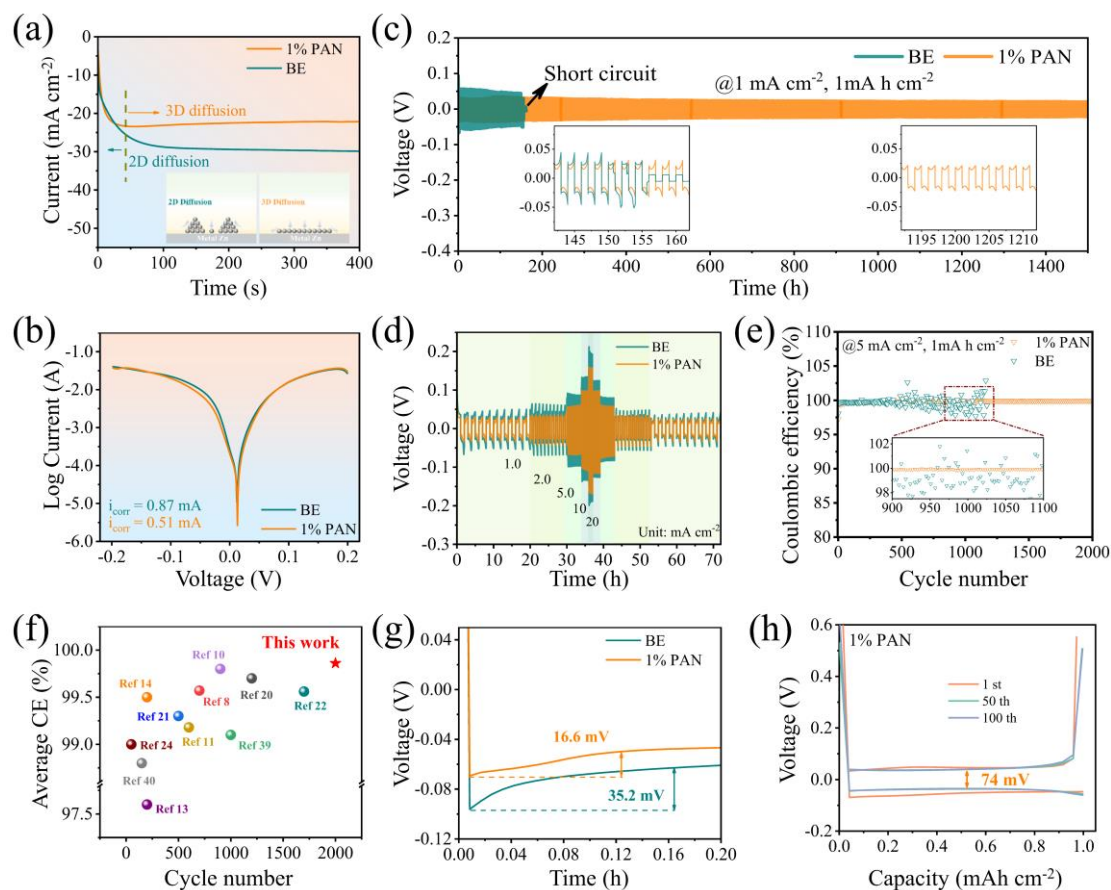


Fig. 2. Electrochemical performance. a) Chronoamperometry test for the diffusion behavior of zinc ions. b) Tafel plots of electrolytes and the calculated corrosion current. c) Long-term performance of Zn|| Zn symmetric batteries on 1 mA cm^{-2} , 1 mA h cm^{-2} . d) Rating performance with a current-density range from 1 to 20 mA cm^{-2} and e) Coulombic efficiency with a Zn|| Cu asymmetric battery on 5 mA cm^{-2} , 1 mA h cm^{-2} . f) A comparison of the average Coulombic efficiency between our results and those reported in previous literature. g) Nucleation overpotential of Zn^{2+} at 1 mA h cm^{-2} . h) Voltage-capacity curves at different cycles with the PAN additive.

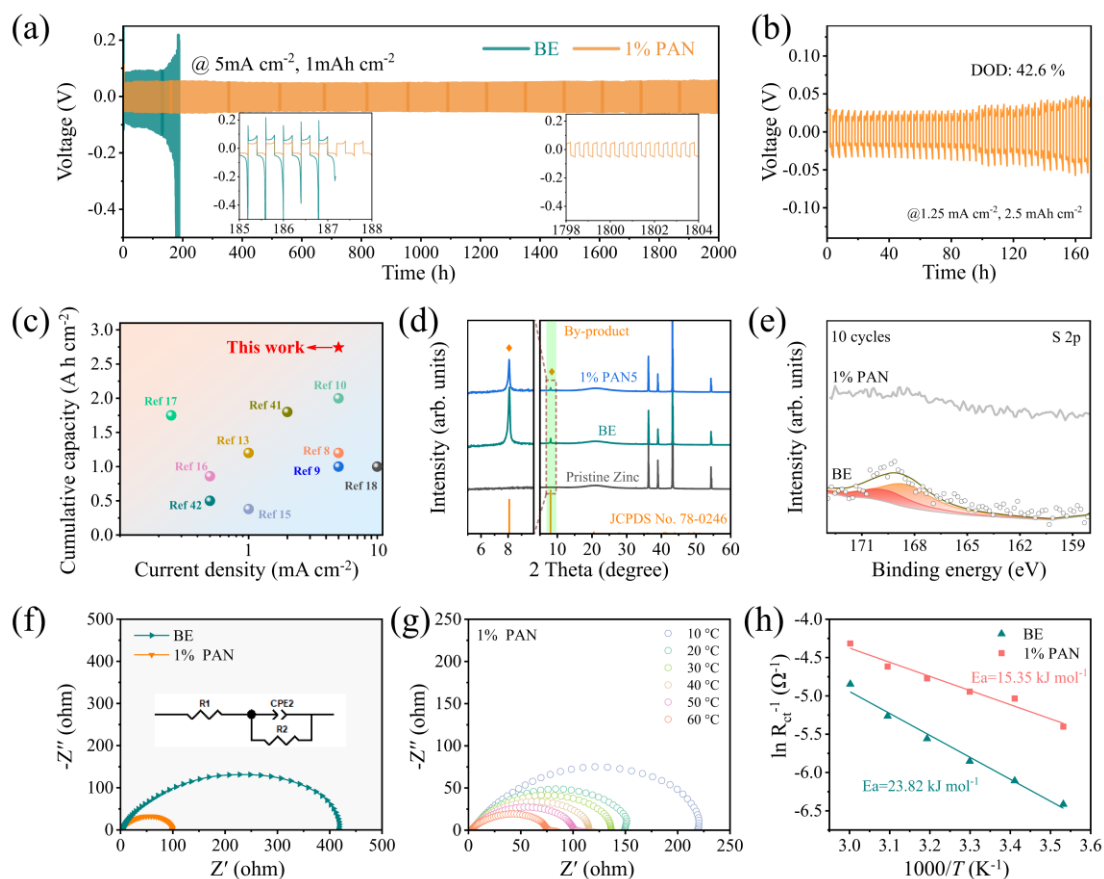


Fig. 3. a) Long cyclic test at 5 mA cm^{-2} , 1 mAh cm^{-2} . b) Depth of discharge test on 1.25 mA cm^{-2} , 2.5 mAh cm^{-2} with a symmetric battery. c) A comparison of cumulative capacity with results reported in previous studies. d) XRD patterns of the zinc metal anode after 10 cycles at 1 mA cm^{-2} . e) Fine spectra of S 2p of the electrodes. f) Nyquist plots of a Zn|| Zn symmetric battery before cycling, and g) Electrolyte with the additive at various temperatures. h) Arrhenius curves of Zn|| Zn batteries at different temperatures.

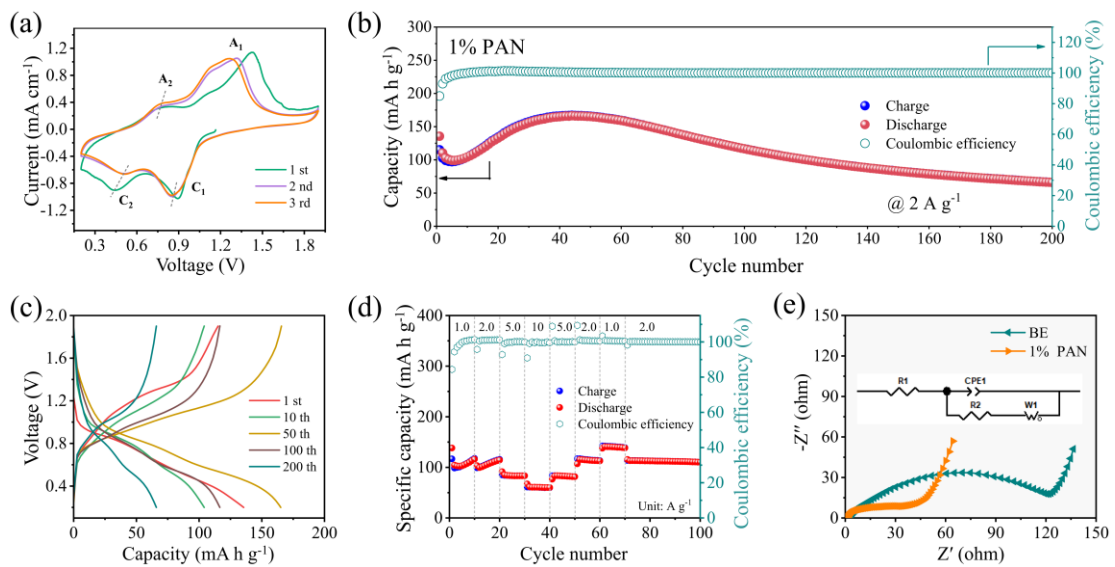


Fig. 4. a) Cyclic voltammograms of the first three cycles with a full battery of Zn||V₂O₅. b) Long cyclic performance at 2 A g⁻¹. c) Charge and discharge profiles at different cycles. d) Rate capabilities at the current densities of 1, 2, 5, and 10 A g⁻¹. e) EIS results of a Zn||V₂O₅ full battery before cycling.

Supporting information for

Zincophilic armor: Phytate ammonium as a multifunctional additive for enhanced performance in aqueous zinc-ion batteries

Fangyuan Xiao^{a,b}, Xiaoke Wang^{a,b}, Kaitong Sun^a, Qian Zhao^a, Cuiping Han^{b,*}, and Hai-Feng Li^{a,*}

^aInstitute of Applied Physics and Materials Engineering, University of Macau, Avenida da Universidade, Taipa, Macao SAR 999078, China

^bFaculty of Materials Science and Energy Engineering/Institute of Technology for Carbon Neutrality, Shenzhen Institute of Advanced Technology, Chinese Academy of Sciences, Shenzhen Guangdong 518055, China.

*Email addresses: cp.han@siat.ac.cn (C. Han)
haifengli@um.edu.mo (H.-F. Li)*

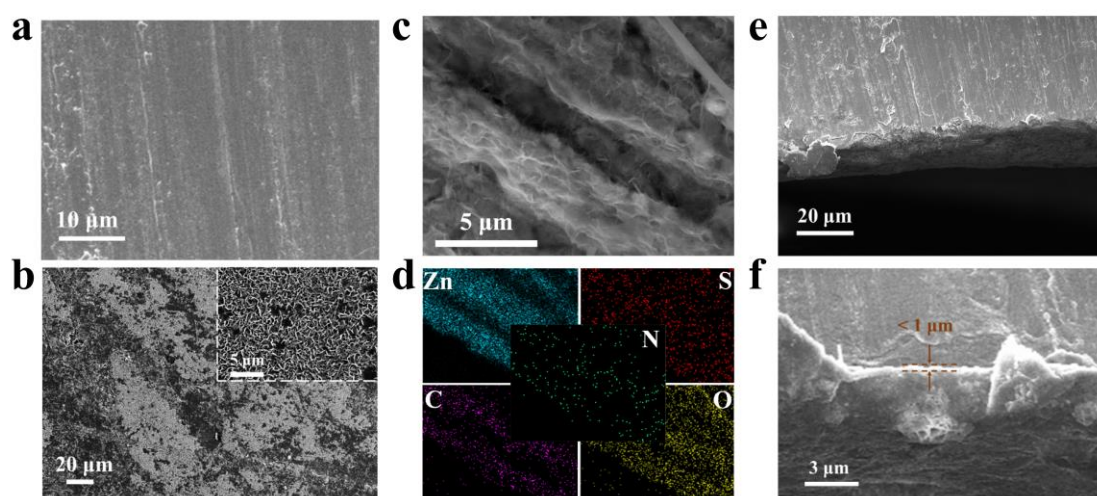


Figure. S1. SEM images of a) Bare zinc metal foil, b) Electrode paired with bare 1 M ZnSO₄ electrolyte after aging for 20 hours. c) Electrode with additive, and d) corresponding EDS mapping results. Cross-sectional images of the electrode: e) with bare electrolyte and f) with additive after 10 cycles at 1mA cm⁻², 1mA h cm⁻².

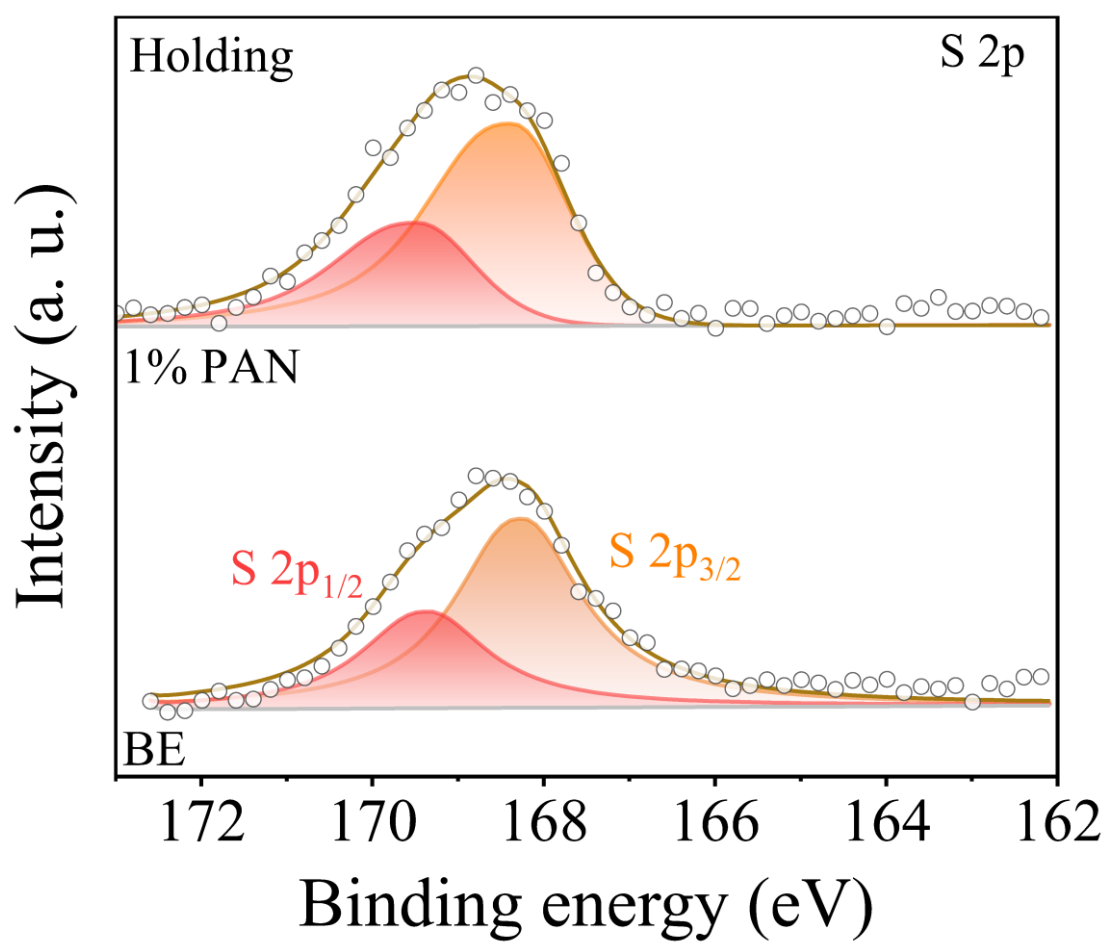


Figure. S2. Fine spectra around S 2p edge with XPS survey.

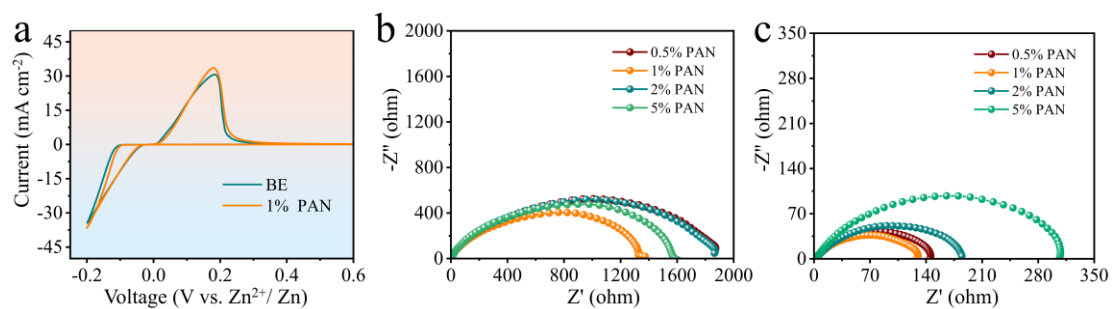


Figure. S3. a) Cyclic voltammetry (CV) curves of the cells before and after the addition of the additive with Zn||Ti asymmetry battery at a scan rate of 1 mV s⁻¹. b) Electrochemical impedance spectra results with different amounts of Zn||Zn symmetric battery assembled initially, and c) after 24 hours of aging.

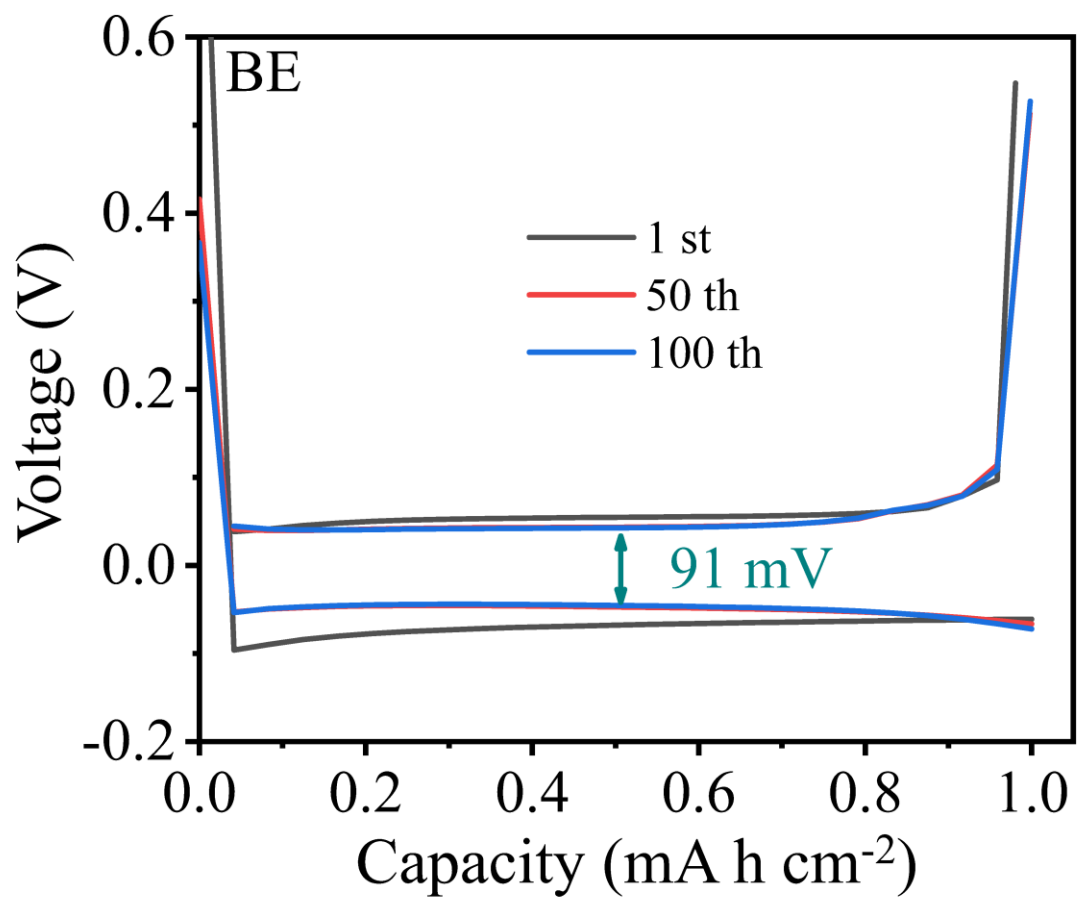


Figure. S4. Voltage- capacity curves on different cycles of bare electrolyte.

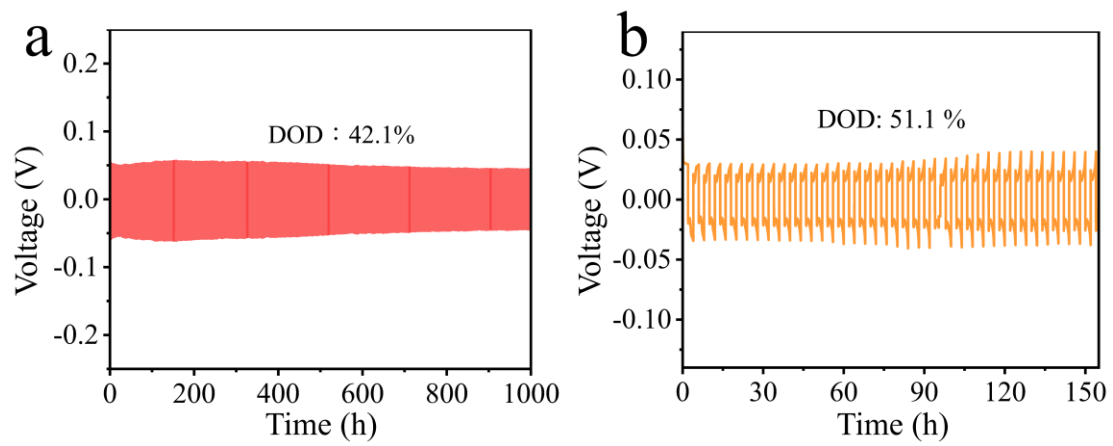


Figure. S5. Depth of discharge (DOD) test. a) DOD ~ 42.6%. b) DOD~ 51.1%

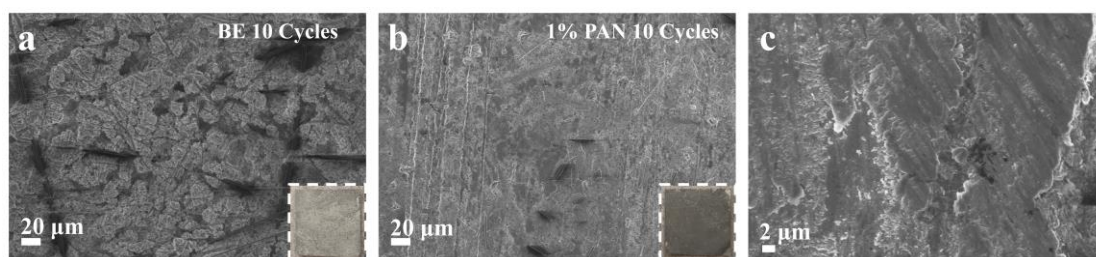


Figure. S6. Optical image (insertion) and SEM images of Zinc metal anode after 10 cycles at 1 mA cm^{-2} , 1 mA h cm^{-2} . a) Bare electrolyte. b) With 1% volume PAN additive. c) High-magnification images of the sample with additive.

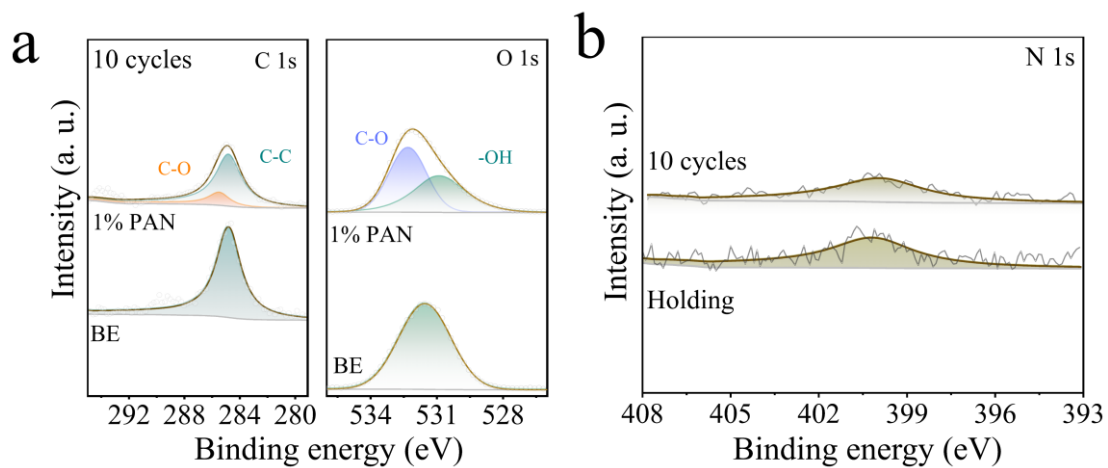


Figure. S7. XPS survey of the electrode. a) C 1s and O 1s edges before and after addition after 10 cycles at 1 mA cm^{-2} , 1 mA h cm^{-2} . b) N 1s spectra after aging with 10 cycles.

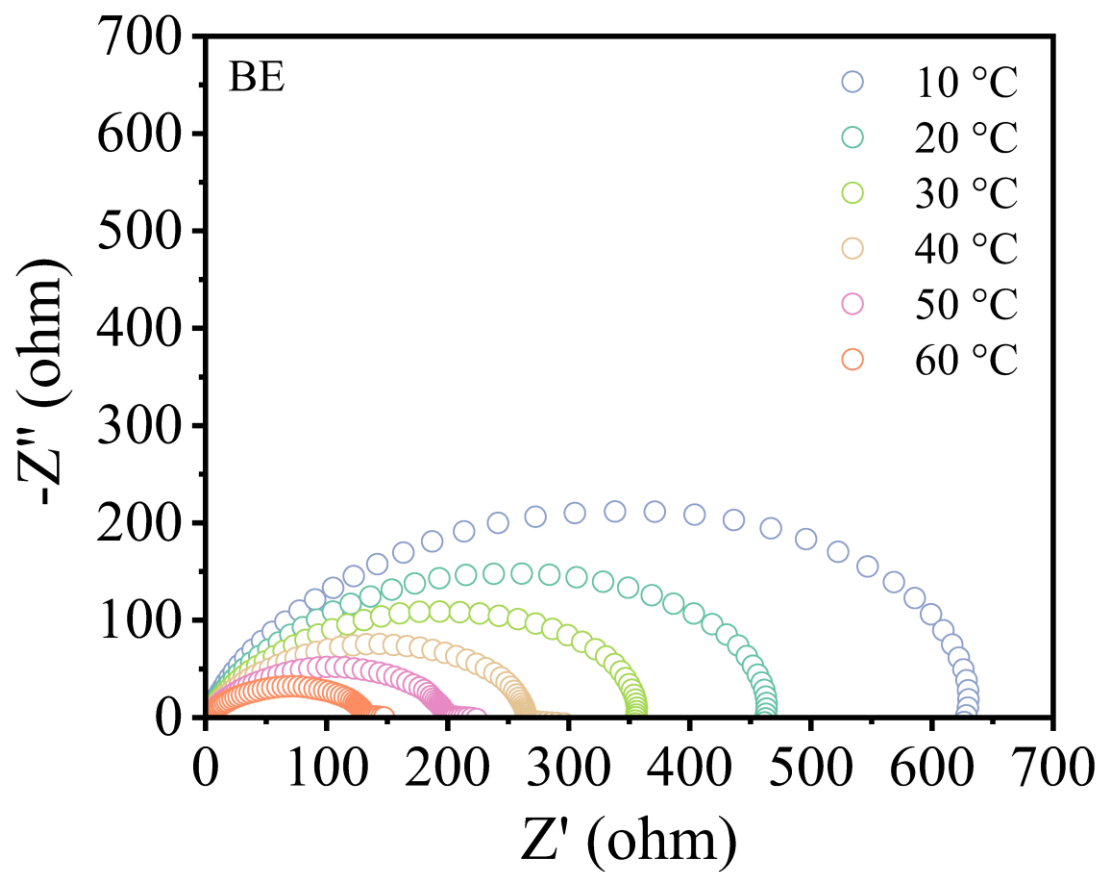


Figure. S8. Electrochemical impedance spectra (EIS) of bare electrolyte from 10 to 60 °C before cycling.